

Mechanisms and Computational Design of Multi-Modal End-Effector with Force Sensing using Gated Networks

Yusuke Tanaka^{1*}, Alvin Zhu^{2,3*}, Richard Lin³, Ankur Mehta³ and Dennis Hong¹

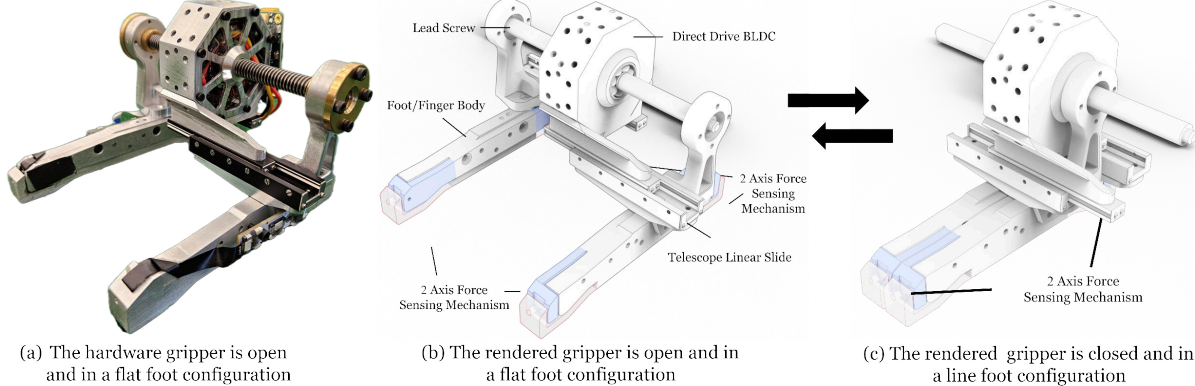


Fig. 1: MAGPIE Hardware and Design Rendering in an isometric view.

Abstract—In limbed robotics, end-effectors must serve dual functions, such as both feet for locomotion and grippers for grasping, which presents design challenges. This paper introduces a multi-modal end-effector capable of transitioning between flat and line foot configurations while providing grasping capabilities. MAGPIE integrates 8-axis force sensing using proposed mechanisms with hall effect sensors, enabling both contact and tactile force measurements. We present a computational design framework for our sensing mechanism that accounts for noise and interference, allowing for desired sensitivity and force ranges and generating ideal inverse models. The hardware implementation of MAGPIE is validated through experiments, demonstrating its capability as a foot and verifying the performance of the sensing mechanisms, ideal models, and gated network-based models.

I. INTRODUCTION

The field of limbed robotics, which uses its limbs as both arms and legs, has seen significant growth in recent years thanks to their multi-modal capabilities. Limbed robots can interact with objects without a dedicated manipulation arm [1], can traverse various complex terrains [2] and uneven surfaces [3], and can climb over obstacles [4]. These abilities expand beyond traditional legged robots' applications, such as search and rescue [2] or planetary exploration [5].

However, the multi-modal nature of limbed robotics presents challenges for end-effector designs since they need to act as both feet for locomotion and grippers for manipulation. As a foot, passive and mechanical compliance

introduces challenges in legged robot attitude controls since they are not actively controllable [6]. Contact detection and contact force sensing play a significant role in the legged robot's locomotion [7]. Grasping force measurements enable both limb movement and grasping to be force-controlled, allowing for more compliant motions [8], [9]. A 6-axis force/torque (F/T) sensor is commonly employed on the ankle, such as in [6]. However, compact force sensors are essential when the sensor cannot be positioned on the ankle or when tactile information from the foot is required for a specific task. [10]. Particularly for highly dynamic bipedal robots, narrow and line feet are more suitable since the contact dynamics and modeling are simplified [11]. However, the line foot design has limited space for contact sensors and is inherently unstable in static and quasi-static cases. These challenges motivate a new end-effector design that can realize multiple configurations while achieving high degrees of force sensing.

Hence, we present MAGPIE (Multi-modal Adaptive Gripper for multi-Pedal Impact-resilient End-effector), a two-finger parallel gripper that functions as a multi-modal foot with an integrated 8-axis force sensing. MAGPIE can transition between flat and line foot configurations with grasping capabilities, providing adequate modality for limbed robotics that necessitates contacting and grasping end-effectors. Our framework optimizes sensing mechanism design, accounting for noise and generating inverse models. Our main contributions are:

- Developing MAGPIE: a parallel grasping end-effector capable of realizing flat and line foot configurations for limbed robotics.
- Computational design framework for 3D hall effect sensor-based 8-axis force sensing mechanisms.

¹Y. Tanaka and D. Hong are with the Department of Mechanical and Aerospace Engineering, UCLA, Los Angeles, CA, USA.

²A. Zhu is with the Department of Computer Science, UCLA, Los Angeles, CA, USA. ³R. Lin and A. Zhu are with the Electrical and Computer Engineering Department, UCLA, Los Angeles, CA, USA. {yusuketanaka, alvister88, richardlin, mehtank, dennishong}@g.ucla.edu. *Y. Tanaka and A. Zhu assert joint first authorship.

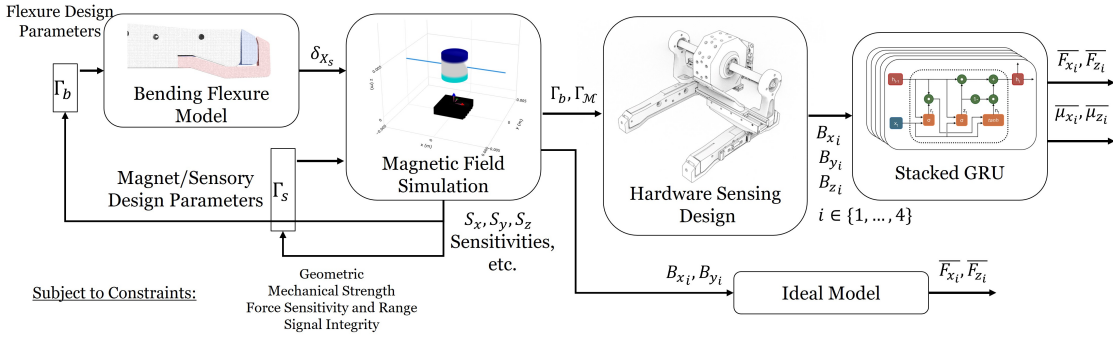


Fig. 2: Computational design framework for the hall effect-based multi-axis force sensing overview. The framework simulated the sensing to design for a desired sensitivity and force range. The framework generates an ideal model using Gaussian radial basis functions. A gated recurrent unit is employed to improve the force measurements and provide uncertainty in the sensing, such as an external significant magnetic field.

- verification of hardware MAGPIE design, sensing mechanisms, and the sensing models.

II. RELATED WORKS

A. Grasping End-Effector as a Foot

Gripping and grasping end-effectors have been developed to improve foot traction on challenging terrains, to grasp, adhere, and climb on objects, and to enable locomotion and manipulation with the same end-effector. Adhesion types of grasping mechanisms such as magnetic [12], suction [13], and gecko [14] are common mechanisms for legs and grasping. Although these adhesive types are designed for relatively flat surfaces, they could be installed on fingers [15]. The granular jamming-based end-effector, conventionally used for grasping objects through its variable compliance [16], has improved the legged robot tractions over various natural terrains [17]. This passive adaptation limits control over end-effector geometry, and adding contact sensors is a non-trivial task. Multi-fingered grippers with spine contact surface [18] can grasp objects or terrains, while the spine needles improve microscale contacts with rough rocky surfaces [19], [20]. However, this type of high degree of freedom (DoF) grippers are less suitable as a foot end-effector for dynamic locomotion and are meant for quasi-static locomotion. A multi-modal gripper can grasp a rock and transform it into a wheel for rover locomotion [21]. The GOAT gripper [22] has two linear flat fingers and has been effective for climbing and quadruped locomotion, but exhibits structural compliance, and the foot is too narrow to stand on statically. Hence, it was not suitable for bipedal locomotion [23].

Therefore, the MAGPIE end-effector aims to achieve grasping capability, while being statically and dynamically suitable as a contacting foot end-effector, such as flat and line foot configurations. The grasping mechanism is designed to be relatively rigid to reduce the control complexity in the limbed robot [6].

B. Force, Contact, and Tactile Sensing on end-effectors

Single and multi-axis F/T sensors are common choices used in legged robots [24], [25]. These sensors typically consist of strain gauges to measure deflections caused by applied forces [8]. However, multi-axis F/T sensors designed

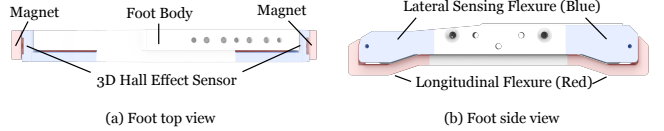


Fig. 3: The force sensing mechanism configuration in the hardware. The red and blue flexures are for ground contact and grasping force sensing, respectively. The magnet is attached on the longitudinal, and the sensor is on the lateral side to better isolate the impact forces from the sensor.

for the large force and torque ranges required by adult-sized humans are often too large to fit in confined space [10]. Tactile skin sensors, such as arrays of strain gauges or those based on vision cameras [26], are designed for more precise manipulation tasks but tend to be less durable. Acoustic and viscous flow tactile sensors offer greater durability and a relatively higher range of tactile force sensing [27], though they are limited by the use of audible signals, restricting their use in certain environments. Multi-modal foot with acoustic, tactile, and capacitive sensors [28] has been effective in obtaining high dimensional sensing with adaptability for an adult-size bipedal robot, though their focus is on rough terrain classification and locomotion. hall effect sensor-based force sensing mechanisms have been explored for more than 2-axis [29] and [30]. However, the multi-axis hall effect sensing mechanism should be designed to generate proper magnetic field changes at the sensor [31], which requires simulation or empirical testing.

MAGPIE overcomes these limitations by employing four three-axis hall effect sensors that detect ground reaction and grasping forces at the edges of each finger, totaling 8-axis force sensing per gripper. Due to magnetic field sensing's nonlinearity, we introduce a computational design framework to search for various design parameters. This framework also generates an idealized inverse sensing model.

III. HARDWARE DESIGN

A. Foot and Finger Design

MAGPIE fingers have to be sensitive to both grasping and ground reaction forces. Three-axis hall effect sensors have been integrated with compliant mechanisms to allow multi-axis force measurements [30]. However, MAGPIE fingers

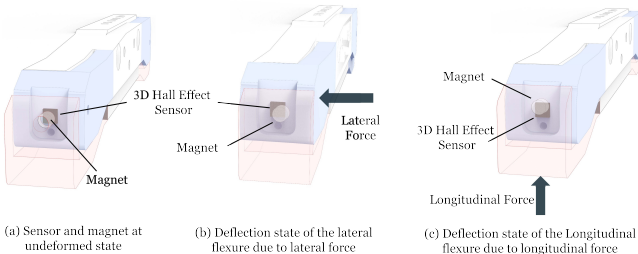


Fig. 4: Sensor and magnet placements, and deflection state with forces.

withstand grasping, ground contact, and repeated impact forces. Thus, a 3-axis hall effect sensor is attached to a one-axial flexure base, and the magnet is installed on the orthogonal axial flexure base as shown in Fig. 3. This design avoids having multiple DoF serial motions, increasing the load capacity and allowing independent compliance tuning for each axis. The hall effect sensor is on the lateral side, i.e., for measuring grasping force, and the magnet is on the longitudinal side, i.e., for measuring ground reaction force. This helps to isolate the electric components and their wires from the landing impact. This design still allows the measurement of two axes simultaneously. Fig. 4 illustrates the force sensing mechanisms at Fig. 3a a nominal state, Fig. 3b a deflected state due to lateral force, and Fig. 3c a deflected state due to longitudinal force.

B. The Gripper Actuation Mechanisms

The MAGPIE's actuation mechanism has to withstand unconventional longitudinal stress due to the ground contact. Hence, we opt for a miniature crossed-roller linear rail system actuated with a BLDC motor. The lateral force sensing flexure is designed to be more sensitive, but once the gripper is closed, the lateral sensing mechanism is not exposed and hence protected. The right and left-handed lead screws are connected at the BLDC inner rotor using MechaLock to distribute torque transfer stress evenly.

C. Circuitry and Sensors

The electronics of the MAGPIE gripper, shown in Fig. 5, are designed to be modular and self-contained, allowing for straightforward integration with the rest of the robotic system. The electrical circuit boards are developed using the hardware description language, Polymorphic Blocks [32] and its human-computer interface [33], which enables schematic, component-level design, electrical modeling, and design verification programmatically. The MAGPIE PCB board integrates a BLDC motor, a 6-axis inertial measurement unit (IMU), an RGB camera, a current/voltage sensor, a color touch display, DC-DC converters, and interfaces via UART and CANbus. The IMU and the cameras will benefit the future end-effector state estimation and visual servo. The four 3-axis hall effect sensors are mounted on custom flexible PCBs with stiffers to simplify sensor placement and reduce hardware complexity. This flexible PCB design minimizes wiring and potential points of failure, improving sensor reliability and ease of installation in MAGPIE.

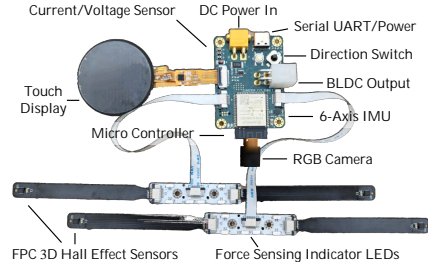


Fig. 5: Circuitry and sensors of the MAGPIE control unit.

IV. SENSOR MODEL AND DESIGN FRAMEWORK

The flexure design, magnet characteristics, 3D hall effect sensors, and magnet placements are vital in MAGPIE contact and tactile force sensing. Hence, these designs require a design framework to determine the appropriate design parameters to achieve proper force sensing range, sensitivity, repeatability, and insensitivity to disturbance.

A. Flexure Analytical and Simulation Model

Here, we employ Von Kármán beam theory to estimate the flexure responses to external forces analytically. While the Euler-Bernoulli beam theory is valid for small deformations, capturing both horizontal and vertical deformations in this design is essential, as the sensor is sufficiently sensitive to detect these effects. The Von Kármán beam theory is suited for describing the large deflections of slender beams by accounting for both bending and in-plane stretching. For the vertical force balance (bending equation), we have:

$$EI \frac{d^4 w(x)}{dx^4} = q(x) - \frac{d}{dx} \left(N(x) \frac{dw(x)}{dx} \right) \quad (1)$$

Where EI represents the flexural rigidity, E is Young's modulus, and I is the second moment of the area of the beam. $w(x)$ denotes the vertical deflection of the beam at a position x along its length. $N(x)$ is the axial force in the beam, and $q(x)$ represents the distributed transverse load per unit length.

For the horizontal force balance (stretching equation):

$$\frac{d}{dx} \left(EA \frac{du(x)}{dx} \right) = \frac{1}{2} EI \left(\frac{dw(x)}{dx} \right)^2 \quad (2)$$

Here, $u(x)$ is the horizontal displacement (in-plane stretching) at position x , and A is the beam's cross-sectional area.

When the axial force $N(x)$ is negligible, (1) simplifies bending equation as:

$$EI \frac{d^4 w(x)}{dx^4} = P \cdot \frac{L - x}{L} \quad (3)$$

The beam edge's angle is derived from the slope of the deflection curve, $w(x)$. The derivative, $\frac{dw(x)}{dx}$, gives the slope at any point along the beam. Using the expression for the second derivative of $w(x)$, the slope at the edge can be obtained as:

$$\theta_{\text{edge}} = \frac{dw(L)}{dx} = \int_0^L \frac{P \cdot (L - x)}{EI} dx \quad (4)$$

B. Magnetic Sensor Signal Model

A computational model and estimate of the sensor signal are vital steps in designing a desired hall effect sensor-based force sensing system. Sensor signal patterns differ based on the magnet's magnetization strength, polarity, sizes, and relative placement with respect to the sensor. Here, we consider cylindrical magnets due to their wider size availability, and the cube or spherical magnets do not affect the signal patterns at micron-scale motion sensing as shown in Fig. 6a. The magnetic field change sensitivity, \mathcal{S} , is a rate of the magnetic field change at the sensor frame due to the magnet motion, denoted as $\mathcal{S} = \frac{\delta B}{\delta X}$. The higher sensitivity can translate to the relatively minor deflection of the beam to generate a larger change in the magnetic field at the sensor. This allows us to design the sensing mechanisms with appropriate force resolution, although the hall effect sensors' sensitivity is set. The magnetic field numerical simulation is implemented using Magpylib [34].

C. Magnetic Interference and Uncertainty

The force sensing is sensitive to magnetic interference. The following are the major sources. 1) Earth's magnetic field, 2) sensor and magnet misalignment, 3) nearby permanent magnet, i.g., another sensor magnet when the gripper is closed, and 4) permanent magnet inhomogeneity.

Conventionally, the external magnetic field interference can be conveyed by having a significantly stronger permanent magnet for the sensor [29]. Here, we incorporate the model to determine the design parameters, changing the mechanism design parameters to mitigate the expected disturbances.

1) *Earth's magnetic field*: The Earth's magnetic field causes background noise, which depends on the orientation of the sensors. However, this field strength is approximately $0.5 \mu\text{T}$, whereas N32 grade NdFeB magnets are 1.2 T . Hence, the effect is negligible where the sensor is placed in proximity to the magnet.

2) *Sensor and magnet misalignment*: The sensor and magnet placements have manufacturing uncertainty, which causes biases and asymmetry in the sensor measurements. Although the biases are relatively more straightforward to calibrate, the asymmetry introduces skew in sensor measurements, albeit the measurement-to-force model becomes distinct for each axis.

3) *Permanent magnet nearby*: In MAGPIE, another permanent magnet can be nearby when the gripper is closed. Although this could be tried to shield or compensate by knowing the gripper finger current distance, our computational framework allows us to design sensing mechanisms that do not affect the measurements more than the desired level at most.

4) *Permanent magnet impurity*: Demagnetization effects in permanent magnets arise from the inhomogeneous response of the magnetic material, leading to a slight weakening of the magnetic field. For NdFeB (neodymium) magnets, the demagnetization effect is typically less than 1% [31].

D. Constraints

1) *Mechanical Constraints*: The sensing mechanism should prevent bending yield stress and fatigue failure. The maximum bending stress is:

$$\sigma_b(x) = \frac{M(x) \cdot c}{I} \quad (5)$$

Where $M(x)$ is the bending moment at position x , c is the distance from the neutral axis to the outermost fiber, and I is the second moment of area. To avoid fatigue failure, the stress amplitude $\sigma_a = \frac{\sigma_{\max} - \sigma_{\min}}{2}$ should correspond to an indefinite fatigue life N_f according to the material's S-N curve.

2) *Geometric Constraints*: In addition to geometric constraints due to the sensor and magnet sizes, the force-sensing range can be limited by having a collision under excessive forces. The sensor survival force range can be increased mechanically by limiting the maximum bending deflection.

3) *Magnetic Signal Integrity Constraints*: The estimated magnetic field strength at the sensor must be within the 3D hall effect sensor range. The possible magnetic disturbances discussed in IV-C introduce uncertainty in the sensing.

E. Force Sensing Model

Estimating contact and grasping forces from 3D hall effect sensor measurements requires inverting the analytical model. Since deriving a closed-form inverse is challenging, numerical and data-driven methods are used in multi-axis force estimation, including inverse FEA [26] and neural networks [29]. We generate an ideal model based on simulated sensor measurements for given applied forces, as illustrated in Fig. 2, and employ Gaussian radial basis functions (GRBF) [35] to model the inverse relationship.

We incorporate real-world data from the MAGPIE hardware to account for uncertainties, such as sensor nonlinearity and hysteresis, not considered in our analytical models. Given the time-dependent nature of hysteresis, we select a stacked Gated Recurrent Unit (GRU) [36], which takes sensor measurements as inputs and outputs estimated mean forces and their uncertainties. Estimating uncertainty is vital to detect unmodeled magnetic field disturbances, such as external magnets, since more significant uncertainty can indicate abnormal operating conditions.

V. RESULTS AND HARDWARE EXPERIMENTS

In this section, we conduct 1) the 3D hall effect sensor-based force sensing mechanism design parameter search through our computational framework. 2) the sensing mechanisms, ideal, and GRU-based sensing model verification and analysis. 3) Testing of the MAGPIE as a gripper and foot.

A. Magent Shapes and Sizes

Fig. 6a shows the magnetic field changes at the sensor for four different magnet shapes. All magnet sizes have a constant minimum bounding box of 2.5 mm, and the tube has a hole diameter of 1 mm. The magnetic field strength varies based on the shape due to differences in the volume.

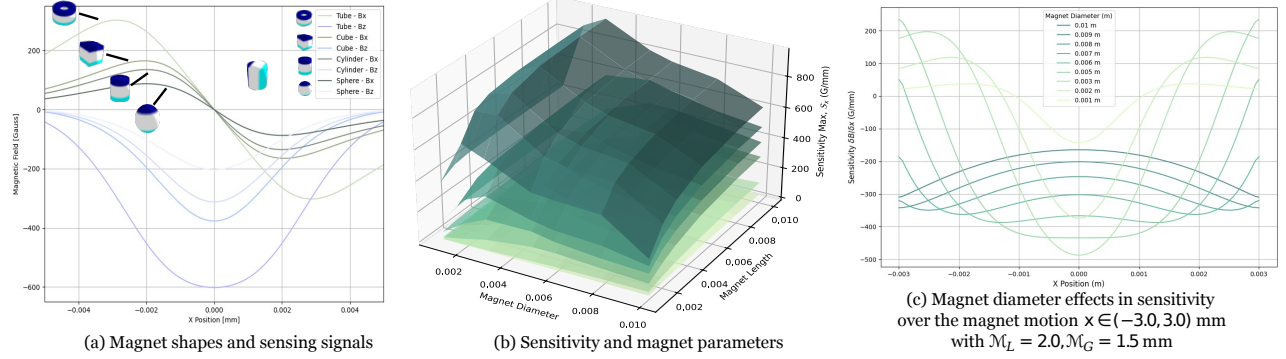


Fig. 6: Simulated magnetic field changes at the sensor frame. The magnets purely move in the x direction. For axial metric magnets, the motion in x and y -axis generates the identical signal.

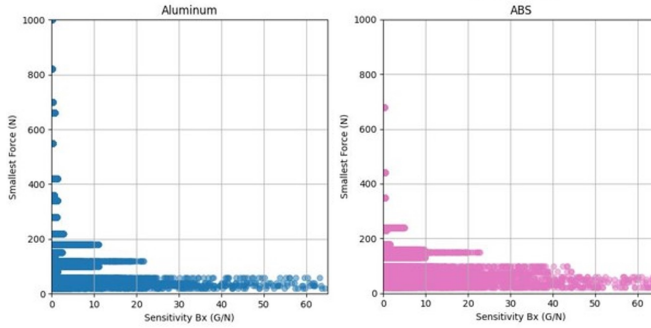


Fig. 7: Parameter sweep results of 10000 design parameters for two different materials, showing one metal and plastic material result.

B. Sensitivity, Magnet Parameters with Self-Interference

Here, using the computational design framework, we simulate the relationship among the maximum sensitivity, $\max(\mathcal{S})$ magnet sizes, and the relative distance to the hall effect sensor. The magnet is moved along with the x axis of the sensor in the range of $(-3.0, 3.0)$ m, and the simulation results in Fig. 6b. The identical size of the magnet is placed at 1.5 mm to represent the case where the gripper is closed, i.e. the closest distance to the other foot magnet.

The maximum sensitivity is proportional to the distance. The longer magnet increases the sensitivity in a log-function manner. The larger diameter magnets do not necessarily increase the sensitivity. Fig. 6c indicates that the sensitivity changes significantly over this magnet x motion. $\mathcal{M}_D = 5.0$ mm exhibits nearly constant sensitivity for $x \in (-0.6, 0.6)$ mm. The larger diameter magnets add nonlinearity in \mathcal{S}_x around $x = 0$ mm. The disturbance due to the neighboring magnets leaked flux in Fig. 6b increases corresponding to \mathcal{M}_d and \mathcal{M}_L . The δB_{x_e} will constantly offset the hall effect sensor measurement given the gripper open or close states.

1) *Sensing Mechanisms Design Search*: Using the entire computational design pipeline, here we analyze the input-output relationships of the applied force and the 3D hall effect sensing with various Γ_b , Γ_M parameters, such as materials and magnet sizing. Fig. 7 plots the possible force sensitivity and the force ranges for different materials. The force sensitivity is affected by both \mathcal{S} in Section. V-B and

the stiffness of the beam. The force range achievable is constrained by the fatigue and bending failure as described in Section. IV-D. Fig. 7 indicates the suitable materials for users' desired force ranges and sensitivity. Both metal and plastic can achieve similar sensing ranges and sensitivity at low ranges (0, 10) Gauss/N, (0, 100) N. In Plastic materials such as ABS, the maximum force range is (0, 200) N. On the other hand, the metal can achieve the force range of 800 N, but the sensitivity is less than $\mathcal{S}_x = 10$ Gauss/N. Parameter sweeping range and resolutions are limited, resulting in sparse distribution for the higher force range in Fig. 7

2) *Design Selection*: Hardware MAGPIE employs A31301 3D linear hall-effect sensors by ALLEGRO Microsystems with a ± 2000 Gauss sensing range and 0.1 Gauss of resolution, which comes with internal compensation such as temperature effects. Through the design search, the beam deflection range was set to 0.5 mm, and the flexure beam was manufactured using wire EDM. The effective beam length, thickness, width were 30, 5 and 15 mm, respectively. Due to the sensor packages and structure limitation, the sensor and the magnet distance \mathcal{M}_G had to be at least 1.5 mm. From Fig. 6c, The magnet $\mathcal{M}_D = 0.003$ m was selected for the highest sensitivity. The sensitivity is nonlinear for the sensing range, which is complex in the coaxial force cases, which is handled through a stacked GRU framework. When the gripper is closed, this mechanism's configuration has less than ± 3 resolutions of A31301 from the simulation.

C. GRBF and GRU Model on Hardware

The ground truth force was recorded using Bota Rokubi force/torque sensors attached to each flexure axis at 100 Hz to determine the relationship between the force applied and the magnetic sensor measurements. Each hall effect sensor has bias calibrated to account for the sensor-magnet misalignment and variances. All four hall effect sensors run at 1000 Hz on board. The GRBF ideal model force estimate is from the simulation in Section. IV-E, which does not incorporate the axis coupling effects. Fig. 8 compares the ground truth applied forces, idea model estimated forces, and the stacked GRU estimated forces with 2-axis and 3-

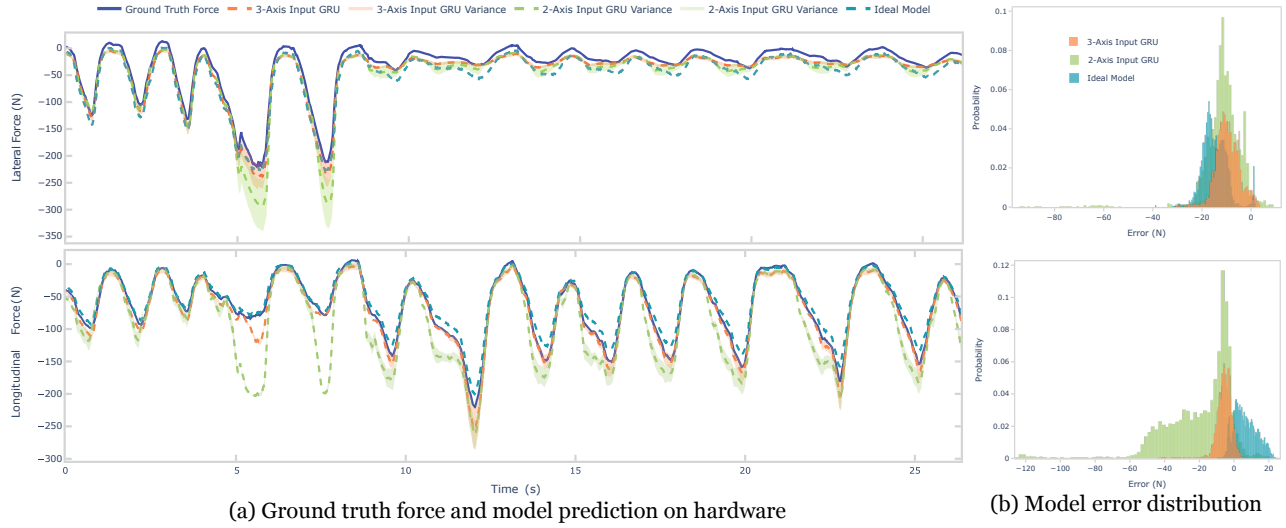


Fig. 8: The ground truth, the ideal model, the stacked GRU with 2-axis and 3-axis inputs.

axis sensor inputs. Each model estimation root square mean error (RSME) and statistical results are listed in Table. I.

A sinusoidal lateral F_x and longitudinal F_z force is applied with varying amplitude with an average frequency of 0.5 Hz as shown in Fig. 8a. The error normalized histogram in Fig. 8b was obtained over the 100 s test. The GRBF ideal model has shown statistical relationships to the hardware sensor-force correlation but underestimates the force at high amplitude. All models showed no statistically meaningful differences in the phase delay in estimation except for 2-Axis GRU F_z . The 2-axis GRU model struggled particularly when both axes experienced significant deviation, such as at 5.7 and 7.7 s. The 3-axis GRU has handled the coupled cases better than the 2-axis GRU with the same amount of data due to additional redundant information indicating the coupling of both axes. The uncertainty estimation increases as the 3-axis GRU deviates significantly from the ground truth, but the uncertainty estimations are low, around zero, regardless of the degree of deviation. Non-uniform normalization may be necessary to improve the variance estimation around zero to force learning in these regions [37].

There were no statistically meaningful deviations in the GRU force estimation due to known magnetic interference, such as from BLDC and when the gripper is closed. The ideal model runs at 11 us, and the GRU takes 22 us on CPU and 15 us on GPU, including data transfer time. The ideal model can be faster if a linear model is used instead. Where an external magnetic field is applied, the GRU uncertainty output consistently increases up to ± 50 N, which can be used to identify the abnormality. This is another essential motivation for adopting GRU instead of the GRBF ideal model, which only provides the mean estimation.

D. Grasping and Foot Capability

Here, we verify MAGPIE's grasping and capability as a foot. MAGPIE employs a custom direct drive BLDC with rated speed and torque of 114 rad/sec and 0.58 N/m

TABLE I: Force sensing errors compared to the ground truth.

	Ideal Model	GRU 2Axis	GRU 3Axis
F_z RMSE [N]	9.2	28.9	7.6
F_z Mean Error [N]	6.7	-20.4	-5.9
F_z Variance [N^2]	6.4	20.5	4.7
F_x RMSE [N]	16.0	15.8	11.0
F_x Mean Error [N]	-15.1	-11.9	-9.8
F_x Variance [N^2]	5.4	10.4	5.1

and peak torque of 0.96 N/m. With the lead screw linear mechanisms, the nominal gripper opening and closing speed of 58.3 mm/sec and the nominal grasping force of 350 N. The rigidity of the entire mechanism was evaluated by applying a static load of 200 N and measuring the deflection, which was 0.3 mm.

VI. CONCLUSION

This paper presented MAGPIE, an end-effector capable of grasping an object while functioning as both line and flat feet with contact/tactile force sensing through 3D hall effect sensors. Our computational design framework and design search enable the design of the sensing mechanisms, including flexure beams, magnet, and sensor parameters, while considering nonlinear effects and magnetic disturbances, such as interference from neighboring sensor magnets when the gripper is closed. MAGPIE mechanisms and force-sensing capabilities have been verified on the hardware using an ideal GRBF model generated from the framework and stacked GRU. MAGPIE enables the development and deployment of limbed robotic systems that can leverage MAGPIE's multi-modality and total 8-axis contact and tactile force sensing for conducting, such as simultaneous locomotion, manipulation, and grasping tasks. Our computational design framework provides a way to further develop hall effect-based force sensing mechanisms that are more resilient and less prone to self-interference. MAGPIE showcased multi-modal robotic end-effectors, promising enhanced versatility in multi-modal robotics.

REFERENCES

[1] F. Shi, T. Homberger, J. Lee, T. Miki, M. Zhao, F. Farshidian, K. Okada, M. Inaba, and M. Hutter, “Circus anymal: A quadruped learning dexterous manipulation with its limbs,” in *2021 IEEE International Conference on Robotics and Automation*. IEEE, 2021, pp. 2316–2323.

[2] K. Hashimoto, S. Kimura, N. Sakai, S. Hamamoto, A. Koizumi, X. Sun, T. Matsuzawa, T. Teramachi, Y. Yoshida, A. Imai *et al.*, “Warec-1—a four-limbed robot having high locomotion ability with versatility in locomotion styles,” in *2017 IEEE International Symposium on Safety, Security and Rescue Robotics (SSRR)*. IEEE, 2017, pp. 172–178.

[3] T. G. Chen, S. Newdick, J. Di, C. Bosio, N. Ongole, M. Lapôtre, M. Pavone, and M. R. Cutkosky, “Locomotion as manipulation with reachbot,” *Science Robotics*, vol. 9, no. 89, p. eadi9762, 2024.

[4] Y. Tanaka, Y. Shirai, A. Schperberg, X. Lin, and D. Hong, “Scaler: Versatile multi-limbed robot for free-climbing in extreme terrains,” *arXiv preprint arXiv:2312.04856*, 2023.

[5] K. Uno, N. Takada, T. Okawara, K. Haji, A. Candalot, W. F. R. Ribeiro, K. Nagaoka, and K. Yoshida, “Hubrobo: A lightweight multi-limbed climbing robot for exploration in challenging terrain,” in *2020 IEEE-RAS 20th International Conference on Humanoid Robots*, 2021, pp. 209–215.

[6] J. Vaillant, A. Kheddar, H. Audren, F. Keith, S. Brossette, K. Kaneko, M. Morisawa, E. Yoshida, and F. Kanehiro, “Vertical ladder climbing by the hrp-2 humanoid robot,” in *2014 IEEE-RAS International Conference on Humanoid Robots*, 2014, pp. 671–676.

[7] K. Walas, D. Kanoulas, and P. Kryczka, “Terrain classification and locomotion parameters adaptation for humanoid robots using force/torque sensing,” in *2016 IEEE-RAS 16th International Conference on Humanoid Robots (Humanoids)*. IEEE, 2016, pp. 133–140.

[8] A. Schperberg, Y. Shirai, X. Lin, Y. Tanaka, and D. Hong, “Adaptive force controller for contact-rich robotic systems using an unscented kalman filter,” in *2023 IEEE-RAS 23rd International Conference on Humanoid Robots*, 2023.

[9] Y. Shirai, X. Lin, A. Schperberg, Y. Tanaka, H. Kato, V. Vichathorn, and D. Hong, “Simultaneous contact-rich grasping and locomotion via distributed optimization enabling free-climbing for multi-limbed robots,” in *2022 IEEE/RSJ International Conference on Intelligent Robots and Systems*. IEEE, 2022, pp. 13 563–13 570.

[10] K. Shinjo, K. Kawaharaduka, Y. Asano, S. Nakashima, S. Makino, M. Onitsuka, K. Tsuzuki, K. Okada, K. Kawasaki, and M. Inaba, “Foot with a core-shell structural six-axis force sensor for pedal depressing and recovering from foot slipping during pedal pushing toward autonomous driving by humanoids,” in *2019 IEEE/RSJ International Conference on Intelligent Robots and Systems (IROS)*, 2019, pp. 3049–3054.

[11] J. Li, J. Ma, O. Kolt, M. Shah, and Q. Nguyen, “Dynamic locomotion manipulation on hector: Humanoid for enhanced control and open-source research,” *arXiv preprint arXiv:2312.11868*, 2023.

[12] T. Bandyopadhyay, R. Steindl, F. Talbot, N. Kottege, R. Dungavell, B. Wood, J. Barker, K. Hoehn, and A. Elfes, “Magneto: A versatile multi-limbed inspection robot,” in *2018 IEEE/RSJ International Conference on Intelligent Robots and Systems (IROS)*, 2018, pp. 2253–2260.

[13] C. Prados, M. Hernando, E. Gambah, and A. Brunete, “Moclora — an architecture for legged-and-climbing modular bio-inspired robotic organism,” *Biomimetics*, vol. 8, no. 1, 2023.

[14] D. Hirano, N. Tanishima, A. Bylard, and T. G. Chen, “Underactuated gecko adhesive gripper for simple and versatile grasp,” in *2020 IEEE International Conference on Robotics and Automation (ICRA)*, 2020, pp. 8964–8969.

[15] H. S. Stuart, M. Bagheri, S. Wang, H. Barnard, A. L. Sheng, M. Jenkins, and M. R. Cutkosky, “Suction helps in a pinch: Improving underwater manipulation with gentle suction flow,” in *2015 IEEE/RSJ international conference on intelligent robots and systems (IROS)*. IEEE, 2015, pp. 2279–2284.

[16] E. Brown, N. Rodenberg, J. Amend, A. Mozeika, E. Steltz, M. R. Zakin, H. Lipson, and H. M. Jaeger, “Universal robotic gripper based on the jamming of granular material,” *Proceedings of the National Academy of Sciences*, vol. 107, no. 44, pp. 18 809–18 814, 2010.

[17] E. Lathrop, I. Adibnazari, N. Gravish, and M. T. Tolley, “Shear strengthened granular jamming feet for improved performance over natural terrain,” in *2020 3rd IEEE International Conference on Soft Robotics (RoboSoft)*, 2020, pp. 388–393.

[18] S. Wang, H. Jiang, T. Myung Huh, D. Sun, W. Ruotolo, M. Miller, W. R. Roderick, H. S. Stuart, and M. R. Cutkosky, “Spinyhand: Contact load sharing for a human-scale climbing robot,” *Journal of Mechanisms and Robotics*, vol. 11, no. 3, p. 031009, 2019.

[19] K. Nagaoka, H. Minote, K. Maruya, Y. Shirai, K. Yoshida, T. Hakamada, H. Sawada, and T. Kubota, “Passive spine gripper for free-climbing robot in extreme terrain,” *IEEE Robotics and Automation Letters*, vol. 3, no. 3, pp. 1765–1770, 2018.

[20] Y. Shirai, X. Lin, Y. Tanaka, A. Mehta, and D. Hong, “Risk-aware motion planning for a limbed robot with stochastic gripping forces using nonlinear programming,” *IEEE Robotics and Automation Letters*, vol. 5, no. 4, pp. 4994–5001, 2020.

[21] M. Uda, K. Sawa, K. Uno, T. Kato, L. T. L. Zheng, and K. Yoshida, “Development and grasping performance evaluation of a wheel-gripper transformable mechanism,” in *The Robotics Society of Japan*. RSJ, 2024, pp. 580–583.

[22] Y. Tanaka, Y. Shirai, Z. Lacey, X. Lin, J. Liu, and D. Hong, “An underactuated whippletree mechanism gripper based on multi-objective design optimization with auto-tuned weights,” in *2021 IEEE/RSJ International Conference on Intelligent Robots and Systems*, 2021, pp. 6139–6146.

[23] Y. Tanaka, A. Schperberg, A. Zhu, and D. Hong, “Scaler-b: A multimodal versatile robot for simultaneous locomotion and grasping,” in *IEEE International Conference on Robotics and Automation @ 40 (ICRA@40)*.

[24] M. Hutter, C. Gehring, D. Jud, A. Lauber, C. D. Bellicoso, V. Tsounis, J. Hwangbo, K. Bodie, P. Fankhauser, M. Bloesch *et al.*, “Anymal—a highly mobile and dynamic quadrupedal robot,” in *2016 IEEE/RSJ international conference on intelligent robots and systems*. IEEE, 2016, pp. 38–44.

[25] A. Schperberg, Y. Tanaka, S. Mowlavi, F. Xu, B. Balaji, and D. Hong, “Optistate: State estimation of legged robots using gated networks with transformer-based vision and kalman filtering,” in *2024 IEEE International Conference on Robotics and Automation (ICRA)*, 2024, pp. 6314–6320.

[26] D. Ma, E. Donlon, S. Dong, and A. Rodriguez, “Dense tactile force estimation using gelslim and inverse fem,” in *2019 International Conference on Robotics and Automation (ICRA)*, 2019, pp. 5418–5424.

[27] M. S. Li and H. S. Stuart, “Acoustac: Tactile sensing with acoustic resonance for electronics-free soft skin,” *Soft Robotics*, 2024.

[28] T. Tyler, V. Malhotra, A. Montague, Z. Zhao, F. L. HammondIII, and Y. Zhao, “Integrating reconfigurable foot design, multi-modal contact sensing, and terrain classification for bipedal locomotion,” *IFAC-PapersOnLine*, vol. 56, no. 3, pp. 523–528, 2023.

[29] D. Jones, L. Wang, A. Ghanbari, V. Vardakastani, A. E. Kedgley, M. D. Gardiner, T. L. Vincent, P. R. Culmer, and A. Alazmani, “Design and evaluation of magnetic hall effect tactile sensors for use in sensorized splints,” *Sensors*, vol. 20, no. 4, p. 1123, 2020.

[30] S. D. M. Nasab, A. Beiranvand, M. T. Masouleh, F. Bahrami, and A. Kalhor, “Design and development of a multi-axis force sensor based on the hall effect with decouple structure,” *Mechatronics*, vol. 84, p. 102766, 2022.

[31] P. Malagò, F. Slanovc, S. Herzog, S. Lumetti, T. Schaden, A. Pellegrinetti, M. Moridi, C. Abert, D. Suess, and M. Ortner, “Magnetic position system design method applied to three-axis joystick motion tracking,” *Sensors*, vol. 20, no. 23, 2020. [Online]. Available: <https://www.mdpi.com/1424-8220/20/23/6873>

[32] R. Lin, R. Ramesh, C. Chi, N. Jain, R. Nuqui, P. Dutta, and B. Hartmann, “Polymorphic blocks: Unifying high-level specification and low-level control for circuit board design,” in *Proceedings of the 33rd Annual ACM Symposium on User Interface Software and Technology*, ser. UIST ’20. New York, NY, USA: Association for Computing Machinery, 2020, p. 529–540. [Online]. Available: <https://doi.org/10.1145/3379337.3415860>

[33] R. Lin, R. Ramesh, N. Jain, J. Koe, R. Nuqui, P. Dutta, and B. Hartmann, “Weaving schematics and code: Interactive visual editing for hardware description languages,” in *The 34th Annual ACM Symposium on User Interface Software and Technology*, ser. UIST ’21. New York, NY, USA: Association for Computing Machinery, 2021, p. 1039–1049. [Online]. Available: <https://doi.org/10.1145/3472749.3474804>

[34] M. Ortner and L. G. Coliado Bandeira, “Magpylib: A free python package for magnetic field computation,” *SoftwareX*, vol. 11, p. p.

100466, 2020. [Online]. Available: <https://www.sciencedirect.com/science/article/pii/S2352711020300170>

[35] G. E. Fasshauer and M. J. McCourt, "Stable evaluation of gaussian radial basis function interpolants," *SIAM Journal on Scientific Computing*, vol. 34, no. 2, pp. A737–A762, 2012.

[36] J. Chung, C. Gulcehre, K. Cho, and Y. Bengio, "Empirical evaluation of gated recurrent neural networks on sequence modeling," 2014. [Online]. Available: <https://arxiv.org/abs/1412.3555>

[37] L. Huang, J. Qin, Y. Zhou, F. Zhu, L. Liu, and L. Shao, "Normalization techniques in training dnns: Methodology, analysis and application," *IEEE Transactions on Pattern Analysis and Machine Intelligence*, vol. 45, no. 8, pp. 10 173–10 196, 2023.